

A simple duty cycle control technique to minimize torque ripple in open-end winding induction motor

Muhammad Zaid Aihsan¹, Auzani Jidin^{2,3}, Azrita Alias^{2,3}, Tole Sutikno^{4,5}

¹Faculty of Electrical Engineering Technology, University Malaysia Perlis (UniMAP), Perlis, Malaysia

²Faculty of Electrical Engineering, Universiti Teknikal Malaysia Melaka (UTeM), Melaka, Malaysia

³Power Electronics and Drives Research Group, CeRIA, UTeM, Melaka, Malaysia

⁴Department of Electrical Engineering, Faculty of Industrial Technology, Universitas Ahmad Dahlan, Yogyakarta, Indonesia

⁵Embedded System and Power Electronics Research Group (ESPERG), Yogyakarta, Indonesia

Article Info

Article history:

Received Nov 7, 2022

Revised Jan 10, 2023

Accepted Jan 23, 2023

Keywords:

Direct torque control

Duty cycle control

Induction motor

Open-end winding

Torque ripple

ABSTRACT

Modern electric vehicles (EVs) that drive an induction motor (IM) fed by a traction inverter are fast gaining popularity due to their simple configuration and robustness. The direct torque control (DTC) technique is one of the best control methods to drive the IM, especially in open-end winding configurations, as it offers more voltage vectors. However, the existence of hysteresis controllers and improper switching technique causes larger torque ripples that leads to variable switching frequency. The study will be focused on the open-end winding induction motor where the direct current (DC) power is fed from both sides of the stator windings using the dual inverter configuration. To minimize the torque ripples, a simple switching technique using the duty cycle control method is proposed by injecting a high-frequency square wave into the default inverter switching status to form the new pattern of voltage vectors. The effectiveness of the proposed technique is tested through MATLAB/Simulink software and validated experimentally with a lab-scale setup using a dSPACE controller. The findings show that the proposed method reduces torque ripple by over 50% while keeping the DTC's simple structure.

This is an open access article under the [CC BY-SA](https://creativecommons.org/licenses/by-sa/4.0/) license.



Corresponding Author:

Muhammad Zaid Aihsan

Faculty of Electrical Engineering and Technology, Universiti Malaysia Perlis

02600 Arau, Perlis, Malaysia

Email: zaid@unimap.edu.my

1. INTRODUCTION

Induction motor (IM) drives are widely utilized in automotive and industrial applications due to their high torque performance and power density. Two different controllers are employed to drive the IM depending on its applications. Scalar control is used for low-performance drive systems, whereas vector control is preferred for high-performance drive systems. Direct torque control (DTC) is a vector control scheme proposed by Takahashi and Noguchi [1] and was based on a hysteresis-based module with several drawbacks, such as high torque ripple and variable switching frequency. By using the hysteresis-based controller, the amount of voltage applied to the stator depends on voltage vectors that are chosen from a lookup table [2]–[9]. The movements of voltage vectors are based on the torque and flux requirements as determined by the hysteresis comparators. The hysteresis band itself has an upper band and lower band limit that allow torque to travel within the area. The faulty selection of the voltage vector will result in a vigorous and uncontrollable movement of torque that leads to overshoot and undershoots within the hysteresis band and causes a large torque ripple and variable switching frequency [10]–[13].

In recent years, various strategies have been presented to address these issues. The easiest method, known as the adjustable hysteresis band, shown in [14]–[16], modifies the hysteresis band size leading to precise torque regulation. However, this method is suitable for small sampling rate devices such as DSP controllers and requires complex hardware arrangement. A DTC system with a dSPACE-based controller runs at a minimum sample rate of $50\mu s$, which causes the torque to rapidly travel between the upper and lower band, leading to overshoot and undershoot unconditionally [17]. The direct torque control space vector modulation (DTC-SVM) method was also investigated [18]–[21]. Along with the advantages of the DTC approach, this methodology assures the inverter switching frequency remains constant while reducing torque ripple. However, this technique is difficult, especially in solving the reference voltage space vector equation. A modern method that combines DTC with predictive control has been getting a lot of attention because it can reduce torque ripple and retain constant switching frequency [22], [23]. However, this system needs the weighting factors to be chosen correctly; otherwise, the torque and flux ripple will be larger. Another study [24]–[26] uses duty cycle control, which uses an active voltage vector for part of a control period and a zero-voltage vector for the rest of the control period. Another new study related to the improvement of dynamic performance in DTC by integrating the supercapacitor as the input voltage for the inverter is covered in [27], [28].

The application of multilevel inverter-fed induction motors has been widely explored, such as three-level cascaded H-bridge inverters (CHMI) [29] and neutral point clamped multilevel inverters (NPCMI) [30]. However, these configurations need to require an additional isolated direct current (DC) voltage supply and capacitors voltage balancing technique which will increase the complexity of the systems. Another topology known as the dual-inverter approach is one of the best topologies as it supplies both sides of the stator windings of the induction motor with the power inverter circuits. This dual-inverter method is best known as direct torque control using an open-end windings induction motor (OEWM). The standard single two-level inverter can produce two-level voltage inversion using six active voltage vectors and two null voltage vectors. Meanwhile, in the OEWM, the voltage inversion can be further increased as it has a wider range of voltage vectors. In OEWM, the possible combinations of voltage vectors are up to 64 voltage vectors which can be divided into short, medium, and long voltage vectors. This feature allows the DTC system to select a proper voltage vector that generates a lower slope of torque regulation for each torque and speed demand.

This paper enhances the previous research in [26] to meet the requirement for a dual-inverter open-end winding system. This technique will minimize the torque ripple by injecting the high frequency of squarewave in the form of duty cycle control and integrating with the inverter switching status of DTC. This approach is straightforward and effective as it improves the torque regulation within the hysteresis band as the new voltage vector is now separated into small pulsations, thus allowing the movement of torque in a zig-zag pattern. This new pattern will prevent the torque from facing the sudden surge movement that might cause the overshoot phenomenon and undershoot condition. The validity of this research is tested using MATLAB/Simulink and verified through experimental setup employing dSPACE 1104 board, and it is evaluated with conventional open-ended DTC technique. In section 2, the proposed structure of DTC is briefly outlined. Section 3 depicts how the torque operates according to the suggested method, and it will cover three types of voltage vectors, namely short, medium and long voltage vectors. Section 4 demonstrates simulation and experimental results for the conventional and proposed techniques. Finally, section 5 provides the findings of this study.

2. THE PRINCIPLE OF DTC USING DUAL-INVERTER TECHNIQUE

The dual-inverter configurations use the base concept of the conventional DTC proposed in [1] with some modifications that satisfy the condition for both inverters. The system still used the default 3-level hysteresis comparator and the 2-level flux comparator but with different definitions of torque and flux calculators and look-up tables that satisfy the condition of inverter 1 and inverter 2. The following equations, which are stated in the stator stationary reference frame, are used to characterize each of the subsystems in the proposed DTC system in terms of space vectors:

$$v_s = r_s i_s + \frac{d\Psi_s}{dt} \quad (1)$$

$$0 = r_r i_r - j\omega_r \Psi_r + \frac{d\Psi_r}{dt} \quad (2)$$

$$\Psi_s = L_s i_s + L_m i_r \quad (3)$$

$$\Psi_r = L_r i_r + L_m i_s \quad (4)$$

$$T_e = \frac{3}{2} p |\Psi_s| |i_s| \sin\delta \quad (5)$$

where p stands for the number of pole pairs, ω_r indicate the rotor electric angular speed in rad/s, L_s , L_r and L_m marks as the motor inductances, and δ is the angle between the stator flux linkage and the stator current space vectors. Based on (1), the d^s – and q^s – axis stator flux in a stationary reference frame may be expressed as:

$$\Psi_{s,d}^s = \int (v_{s,d}^s - i_{s,d}^s r_s) dt \quad (6)$$

$$\Psi_{s,q}^s = \int (v_{s,q}^s - i_{s,q}^s r_s) dt \quad (7)$$

this study will use the standard two-level inverter for the dual-inverter technique. In the same situation as the conventional two-level inverter, the phase voltage across the stator winding of the dual inverter supplied drive can be derived as follows:

$$V_{AA'} = V_{AN} - V_{A'N'} - V_{NN'} \quad (8)$$

$$V_{BB'} = V_{BN} - V_{B'N'} - V_{NN'} \quad (9)$$

$$V_{CC'} = V_{CN} - V_{C'N'} - V_{NN'} \quad (10)$$

where the V_{XN} and $V_{X'N'}$ are the poles, voltage measured at every inverter leg and $V_{XX'}$ is the phase voltage, and X indicates as phase A, phase B, and phase C. The different voltage between two negative rails of DC supplies, also known as common mode voltage, can be written as:

$$V_{NN'} = \frac{1}{3} [(V_{AN} - V_{A'N'}) + (V_{BN} - V_{B'N'}) + (V_{CN} - V_{C'N'})] \quad (11)$$

the (6) and (7) can be expressed in term of switching states S_a^{1+} , S_b^{1+} , S_c^{1+} , S_a^{2+} , S_b^{2+} and S_c^{2+} in a $V_{s,d}^s$ and $V_{s,q}^s$ components of phase voltages.

$$V_{s,d}^s = \frac{V_{dc}}{3} [2(S_a^{1+} - S_a^{2+}) - (S_b^{1+} - S_b^{2+}) - (S_c^{1+} - S_c^{2+})] \quad (12)$$

$$V_{s,q}^s = \frac{V_{dc}}{\sqrt{3}} [(S_b^{1+} - S_b^{2+}) - (S_c^{1+} - S_c^{2+})] \quad (13)$$

The switching states above are labelled using binary system method and can be expressed as (14).

$$S_x^{y+/-} = \begin{cases} 1 & \text{Indicates the upper/lower switch is ON} \\ 0 & \text{Indicates the upper/lower switch is OFF} \end{cases} \quad (14)$$

Where superscript of y indicates the number of inverter 1 or inverter 2 and $' + / - '$ represents the upper side (+) and lower side (-) of switches in each inverter as in Figure 1.

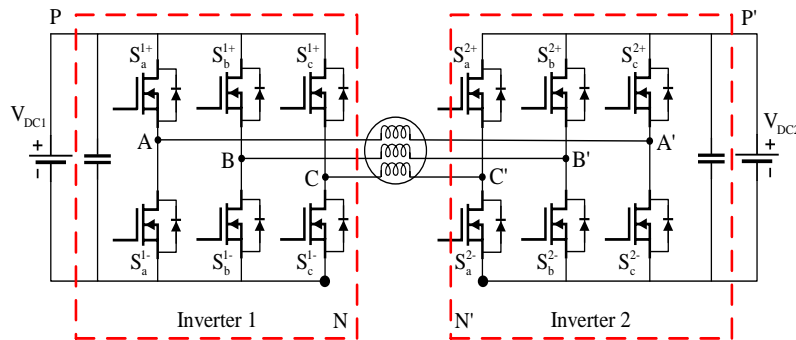


Figure 1. Configuration of open-end winding induction motor supplied using dual-inverters

By using the dual-inverter technique, each inverter has its own voltage vectors. With a proper arrangement and vectors mapping, the possible 64 voltage vectors can be mapped in 4 categories as in Figure 2. The 4 categories namely as short voltage vectors $\vec{v}_{ss,i}$, medium voltage vectors $\vec{v}_{sm,i}$, long voltage vectors $\vec{v}_{sl,i}$ and null or zero voltage vectors, $\vec{v}_{sz,0}$ $\vec{v}_{sz,0}$. The subscript of $'i'$ represents the number of vectors starting from

1 to 6. For example, the short voltage vector of $\bar{v}_{sS,2}$ has 6 combinations and the chosen combination is [000011]. Same situations for the medium voltage vector of $\bar{v}_{sM,4}$ is equal to [010100] and the long voltage vector of $\bar{v}_{sL,3}$ is [110001]. For the null of zero voltage vectors, there is no selection of number for voltage vectors as the superscript will be replace with 0 value. Above 64 vectors, only 20 vectors are chosen and grouped into 18 active voltage vectors and 2 null voltage vectors based on its suitability in terms of the better tangential component to the circular flux locus in each sector definitions.

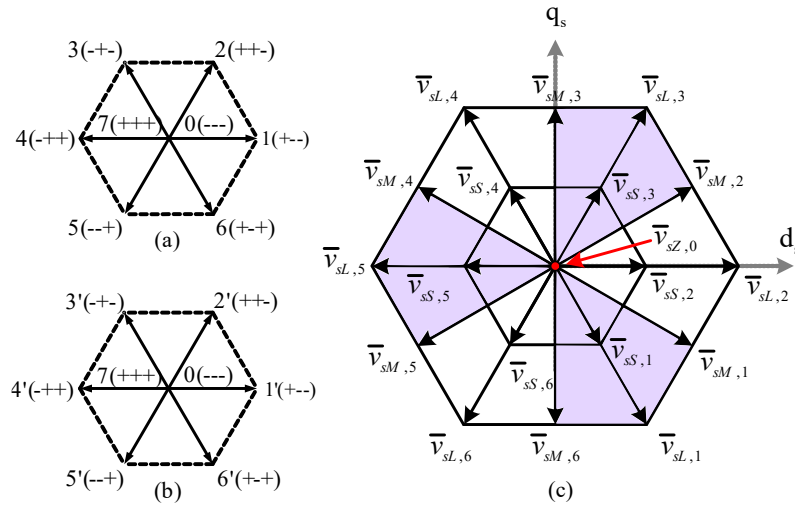


Figure 2. Voltage space vector structure of two-level inverters: (a) for inverter 1, (b) for inverter 2, and (c) combination of 64 voltage vectors

3. OPERATION OF TORQUE USING PROPOSED TECHNIQUE

The proposed technique block is added in the default DTC OEWM as in Figure 3. The technique modifies the conventional inverter switching status into new switching patterns and will not affect the original concept of the DTC system. The basic configuration of DTC OEWM is used, and the information on the inverter switching status from the look-up table, as in Figure 4, will be integrated with the high-frequency signal.

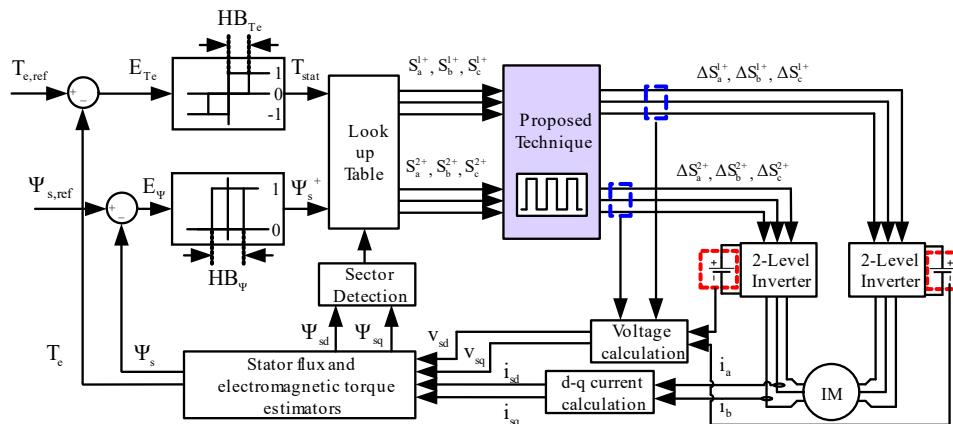


Figure 3. Structure of OEWM DTC with inclusion of proposed technique

The value of 'K' in Figure 4 denotes the constant value that needs to be set to cross the triangular waveform for generating the high pulsation of the square wave in a form of duty cycle. Next, the high pulsation square wave will integrate with the inverter switching of $S_a^1, S_b^1, S_c^1, S_a^2, S_b^2$ and S_c^2 from the look-up table to form the new switching pattern. The NOT-gates on each leg are needed as the inverted gate signals are connected to the lower side of the inverter.

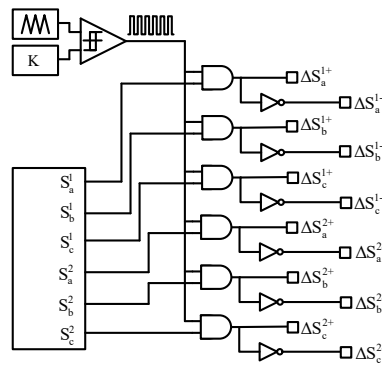


Figure 4. Proposed technique configurations

The following Figure 5 illustrates the behavior of the switching pattern and its effect on the torque performance for both the conventional and proposed technique. The solid black trace represents the conventional technique, and the blue trace is for the proposed techniques. Since the dual-inverter technique can utilize all 64 voltage vectors, thus this DTC system can select various types of voltage vectors between short, medium, and long voltage vectors depending on its demand and conditions of speed. For short voltage vectors, the amplitude of vectors can be indicated by $\sigma_T^+ = +1$, medium vectors, $\sigma_T^+ = +2$ and long vectors, $\sigma_T^+ = +3$. During the conventional technique, the torque is controlled by the default switching states. The condition of torque will be in increment state, T_e^+ remain still until the active voltage vectors, V_s touch the upper hysteresis band, HB_T limit before started to select the zero-voltage vector, $-V_s$, allowing the torque to move in decrement state, T_e^- . Due to this improper control, this torque can easily surge and cause large torque ripples. If the torque crossed the hysteresis band, it would choose reverse voltage vectors to ensure the sudden drop of torque so that it will maintain oscillates at torque reference. When the proposed technique is employed, the voltage vectors are now in a small voltage pulsation between active vectors, ΔV_s and zero vectors, ΔV_o . This pattern will allow the movement of torque can be properly controlled and limit the surge limit. As shown in Figure 5, the proposed technique allows the torque to move in a zig-zag pattern and limits the torque under the reference line (red trace). This advantage enables the DTC system not to generate the reverse voltage vectors, thus helping the torque to move in proper condition resulting in less oscillation and torque ripple disruption.

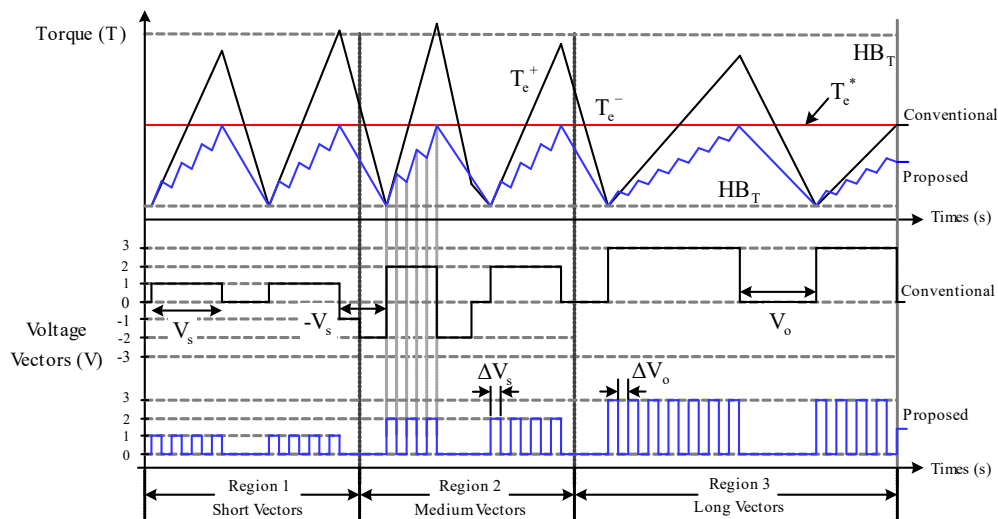


Figure 5. New switching scheme using proposed technique

4. RESULTS AND DISCUSSION

4.1. Parameters and settings

The proposed technique was simulated using MATLAB/Simulink and tested with hardware experimental for validation purposes. The induction motor used in this study with rated torque 4Nm and a flux of 0.8452 Wb. The parameters and specifications used for this experimental setup are shown in Table 1. The complete DTC OEWM, shown in Figure 6, is set up to experimentally verify the proposed switching technique. A dual-inverter with a three-phase configuration drives the induction motor at both windings. This means the induction motor's standard wye or delta connection is open and fed with a power input from the inverter. The induction motor is coupled to the DC motor unit to act as a load and can be adjusted through the DC power supply. The main controller used in this setup is the dSPACE 1104 and the results are captured through the digital oscilloscope Tektronix DPO 3034. The dual inverter is powered up by 200 V in total which mean it is divided equally 100 V at both sides. In this study, the selected value for torque is approximately 2 Nm. The process of capturing the results for both the conventional and proposed techniques is done by triggering the flag signal in the same windows. This technique is implemented for both simulation and hardware and it is important as to see the effectiveness of the proposed technique compared to the conventional method.

Table 1. Induction motor parameters

Parameter		Value
Induction motor	Rated power, P	1.1 kW
	Rated speed, $\omega_{m rated}$	2800 rpm
	Stator resistance, R_s	6.1 Ω
	Rotor resistance, R_r	6.2293 Ω
	Mutual Inductance, L_m	0.4634 mH
	Rotor self-inductance, L_r	0.47979 mH
	Stator self-inductance, L_s	0.47979 mH
	Number of pole pairs, p	2
Speed conditions	Short voltage vectors	300 rpm
	Medium voltage vectors	600 rpm
	Long voltage vectors	900 rpm
Inverter setting	Inverter 1	100 V
	Inverter 2	100 V
	Duty cycle, K	0.5
	Triangular frequency	10 kHz

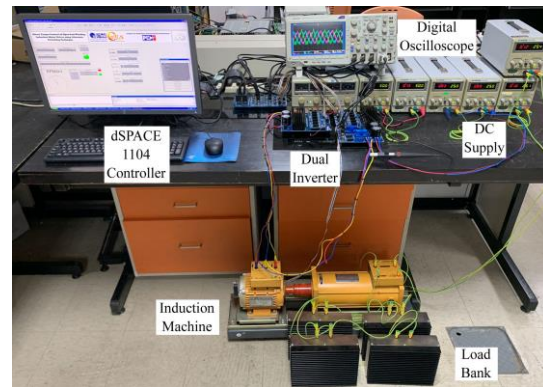


Figure 6. Experimental setup

4.2. Simulation and experimental results

The focus of this study is to observe the performance of torque ripple in the DTC-OEWIM as three types of voltage vectors are utilized. As shown in Figures 7 to 9 are the results for short, medium and long voltage vectors respectively. Each of the results has its full-scale size and a magnified version. Figure 7(a) shows the short voltage vectors employed to drive the induction motor. From the injected 200 V input voltage, the short vectors use 60 V to drive the induction motor. While medium vectors and long vectors utilized 100 V and 160 V, as shown in Figures 8(a) and 9(a). From the figures, it can be observed that each type of voltage vector suffers from high torque ripples during conventional DTC and the torque ripples ramp up over the targeted estimated value 2 Nm. Due to this high ripple, there are many chances of torque to cross the hysteresis band limit, thus allowing the DTC system to select the reverse voltage vectors. Based on Figure 7(b), Figure 8(b), and Figure 9(b) shows that the phase voltage also suffers from massive noises and disturbance.

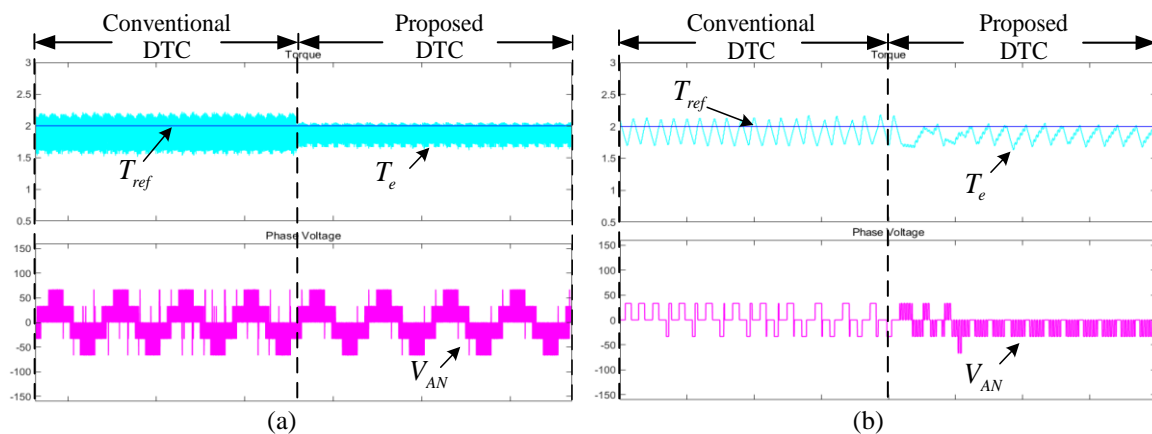


Figure 7. The simulation results of torque and voltage using short vectors (a) full scale and (b) magnified

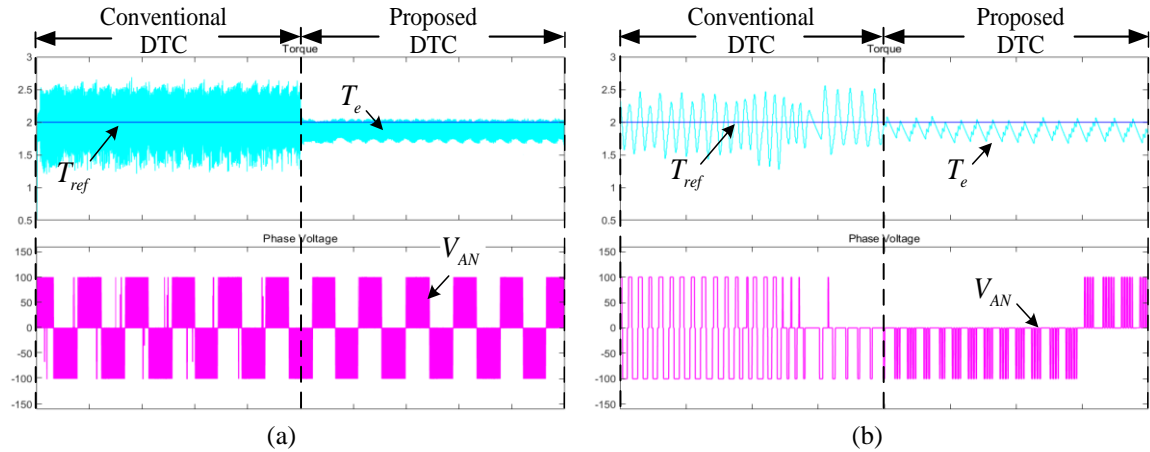


Figure 8. The simulation results of torque and voltage using medium vectors (a) full scale (b) magnified

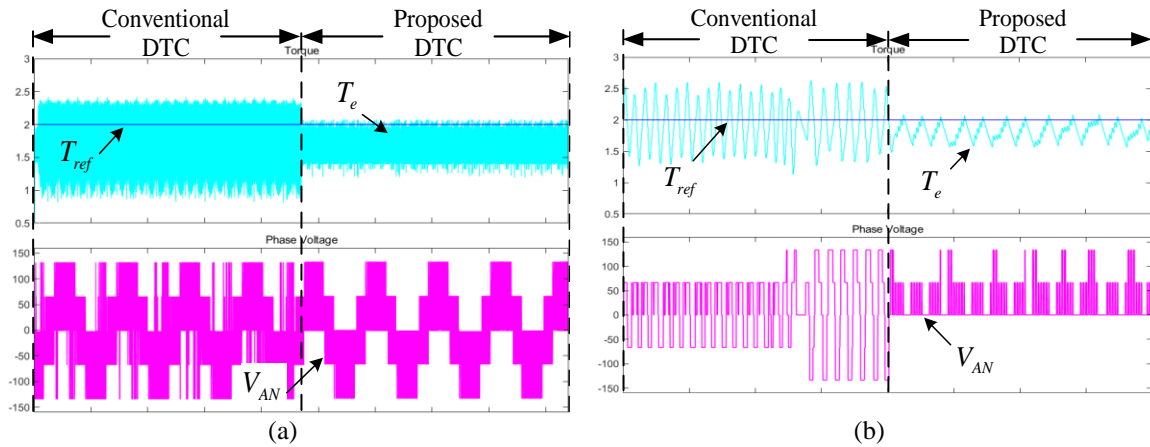


Figure 9. The simulation results of torque and voltage using long vectors (a) full scale and (b) magnified

When the proposed technique is employed, the behavior of torque immediately improves and reduces its ripples. As shown in the magnified version in Figure 7(b), Figure 8(b), and Figure 9(b), the surge torque started to reduce, and the slope formed a linear zig-zag pattern. Furthermore, the increment and decrement of torque are now in a uniform pattern as it is now following the duty cycle pattern from the proposed technique. The condition of phase voltage also improves drastically as the noises from the previous state almost disappear, as shown in Figure 7(a), Figure 8(a), and Figure 9(a). The lab scale DTC OEWM shown in Figure 6 is utilized for experimental results. The same measurement as simulation results where the short, medium, and long voltage vectors are tested with the conventional and proposed technique. Figure 10, Figure 11 and Figure 12 shows the torque performance under short, medium and long-voltage vectors respectively. For short and long, these two voltage vectors shared the same direction but with different magnitudes. It shows both results suffer from high torque ripple at uneven rates during conventional technique and causing frequent selection of reverse voltage vectors as shown in Figure 10(a) and Figure 12(a). While for results that utilize the medium voltage vectors, the torque performance is affected in average ripples, as shown in Figure 11(a). The same situation to phase voltage, where every type of voltage vector suffers in massive noise and frequent selection of reverse voltage vectors. The results started to improve for both torque and phase voltage when the proposed duty cycle technique was employed. The magnified version of torque performance in Figure 10(b), Figure 11(b) and Figure 12(b) started to reduce its surge and move in a uniform pattern following the duty cycle wave pattern. Noticeable that the reverse voltage vectors are not selected in the proposed technique in Figure 10(a), Figure 11(b), and Figure 12(b).

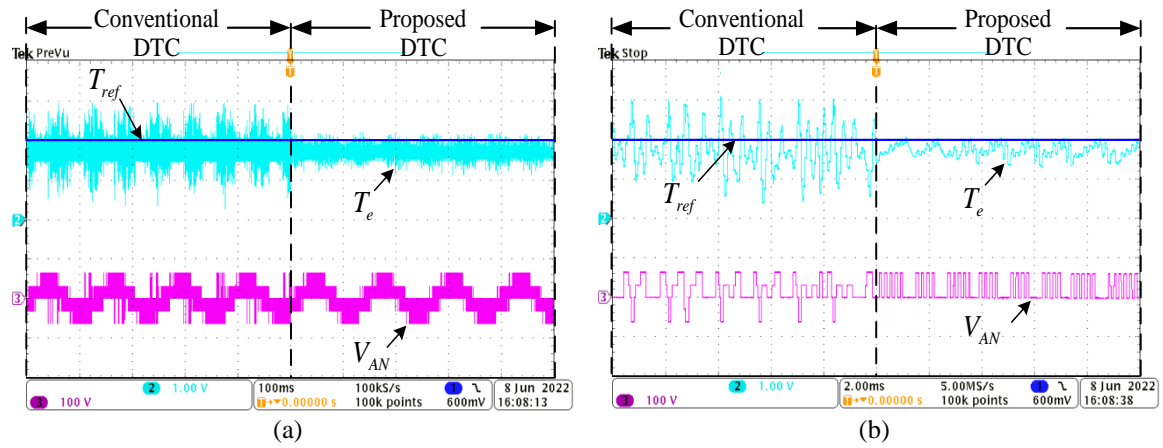


Figure 10. The experimental results of torque and voltage using short vectors (a) full scale and (b) magnified

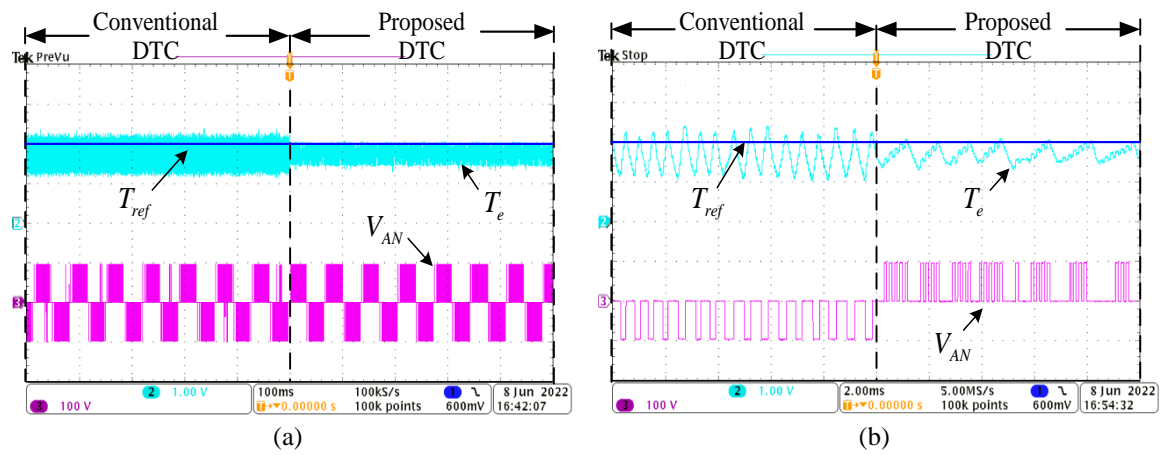


Figure 11. The experimental results of torque and voltage using medium vectors (a) full scale and (b) magnified

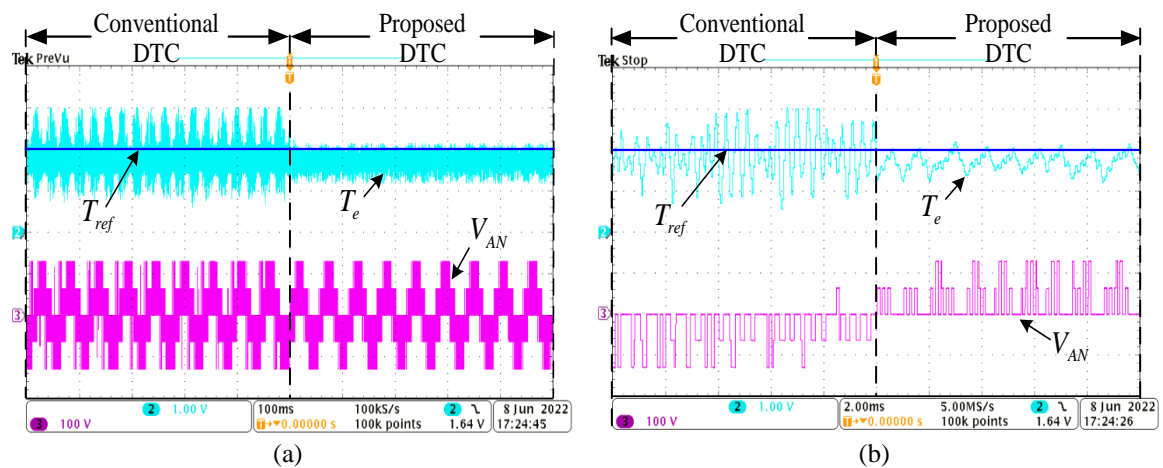


Figure 12. The experimental results of torque and voltage using long vectors (a) full scale and (b) magnified

5. CONCLUSION

A simple and straightforward control method has been proposed to tune the surge torque ripples using a simple duty cycle control integrated with the inverter switching status. The proposed method changes the default inverter switching status into a new pattern of voltage vectors. It allows the torque to be controlled uniformly, thus helping in not selecting the reverse voltage vectors. The movement of torque in a uniform zig-

zag pattern allows the system to work in a proper sequence and not cross the hysteresis band limit. This method is workable for three types of voltage vectors, namely short, medium and long voltage vectors. This method is simple and tune able without changing the default DTC OEWM.




REFERENCES

- [1] I. Takahashi and T. Noguchi, "A New Quick-Response and High-Efficiency Control Strategy of an Induction Motor," *IEEE Transactions on Industry Applications*, vol. IA-22, no. 5, pp. 820–827, 1986, doi: 10.1109/TIA.1986.4504799.
- [2] S. A. A. Tarusan, A. Jidin, and M. L. M. Jamil, "The optimization of torque ripple reduction by using DTC-multilevel inverter," *ISA Transactions*, vol. 121, pp. 365–379, 2022, doi: 10.1016/j.isatra.2021.04.005.
- [3] X. Chen, Z. Zhang, L. Yu, and Z. Bian, "An Improved Direct Instantaneous Torque Control of Doubly Salient Electromagnetic Machine for Torque Ripple Reduction," *IEEE Transactions on Industrial Electronics*, vol. 68, no. 8, pp. 6481–6492, Aug. 2021, doi: 10.1109/TIE.2020.3003596.
- [4] G. H. B. Foo and X. Zhang, "Constant Switching Frequency Based Direct Torque Control of Interior Permanent Magnet Synchronous Motors With Reduced Ripples and Fast Torque Dynamics," in *IEEE Transactions on Power Electronics*, vol. 31, no. 9, pp. 6485–6493, Sept. 2016, doi: 10.1109/TPEL.2015.2503292.
- [5] I. M. Alsofyani and K. -B. Lee, "Improved Transient-Based Overmodulation Method for Increased Torque Capability of Direct Torque Control With Constant Torque-Switching Regulator of Induction Machines," in *IEEE Transactions on Power Electronics*, vol. 35, no. 4, pp. 3928–3938, April 2020, doi: 10.1109/TPEL.2019.2939327.
- [6] N. Yan, X. Cao, and Z. Deng, "Direct torque control for switched reluctance motor to obtain high torque-ampere ratio," *IEEE Transactions on Industrial Electronics*, vol. 66, no. 7, pp. 5144–5152, 2019, doi: 10.1109/TIE.2018.2870355.
- [7] N. R. N. Idris and A. H. M. Yatim, "Direct torque control of induction machines with constant switching frequency and reduced torque ripple," *IEEE Transactions on Industrial Electronics*, vol. 51, no. 4, pp. 758–767, 2004, doi: 10.1109/TIE.2004.831718.
- [8] Y. Luo and C. Liu, "A simplified model predictive control for a dual three-phase PMSM with reduced harmonic currents," *IEEE Transactions on Industrial Electronics*, vol. 65, no. 11, pp. 9079–9089, 2018, doi: 10.1109/TIE.2018.2814013.
- [9] M. Zadehbagheri, T. Sutikno, and M. J. Kiani, "A new method of virtual direct torque control of doubly fed induction generator for grid connection," *International Journal of Electrical and Computer Engineering (IJECE)*, vol. 13, no. 1, p. 1201, 2023, doi: 10.11591/ijece.v13i1.pp1201-1214.
- [10] I. M. Alsofyani and K. B. Lee, "Enhanced Performance of Constant Frequency Torque Controller-Based Direct Torque Control of Induction Machines with Increased Torque-Loop Bandwidth," *IEEE Transactions on Industrial Electronics*, vol. 67, no. 12, pp. 10168–10179, 2020, doi: 10.1109/TIE.2019.2959477.
- [11] M. Magdy, S. Abu-Zaid, and M. A. Elwany, "Artificial intelligent techniques based on direct torque control of induction machines," *International Journal of Power Electronics and Drive Systems (IJPEDS)*, vol. 12, no. 4, p. 2070, 2021, doi: 10.11591/ijpeds.v12.i4.pp2070-2082.
- [12] I. Rkik, M. El Khayat, A. Ed-Dahhak, M. Guerbaoui, and A. Lachhab, "An enhanced control strategy based imaginary swapping instant for induction motor drives," *International Journal of Electrical and Computer Engineering (IJECE)*, vol. 12, no. 2, p. 1102, Apr. 2022, doi: 10.11591/ijece.v12i2.pp1102-1112.
- [13] Q. Al Azze and I. A. R. Hameed, "Reducing torque ripple of induction motor control via direct torque control," *International Journal of Electrical and Computer Engineering*, vol. 13, no. 2, pp. 1379–1386, 2023, doi: 10.11591/ijece.v13i2.pp1379-1386.
- [14] A. A. Kadum, "New adaptive hysteresis band width control for direct torque control of induction machine drives," *International Journal of Power Electronics and Drive Systems*, vol. 11, no. 4, pp. 1908–1917, 2020, doi: 10.11591/ijpeds.v11.i4.pp1908-1917.
- [15] A. N. Abdullah and M. H. Ali, "Direct torque control of im using PID controller," *International Journal of Electrical and Computer Engineering*, vol. 10, no. 1, pp. 617–625, 2020, doi: 10.11591/ijece.v10i1.pp617-625.
- [16] S. Lakhimsetty, V. S. P. Satelli, R. S. Rathore, and V. T. Somasekhar, "Multilevel Torque Hysteresis-Band Based Direct-Torque Control Strategy for a Three-Level Open-End Winding Induction Motor Drive for Electric Vehicle Applications," *IEEE Journal of Emerging and Selected Topics in Power Electronics*, vol. 7, no. 3, pp. 1969–1981, 2019, doi: 10.1109/JESTPE.2018.2870382.
- [17] M. Es-saadi, H. Chaikhy, and M. Khafallah, "Implementation and Investigation of an Advanced Induction Machine Field-Oriented Control Strategy Using a New Generation of Inverters Based on dSPACE Hardware," *Applied System Innovation*, vol. 5, no. 6, p. 106, 2022, doi: 10.3390/asi5060106.
- [18] M. Sellah, A. Kouzou, M. Mohamed-Seghir, M. M. Rezaoui, R. Kennel, and M. Abdelrahem, "Improved DTC-SVM based on input-output feedback linearization technique applied on DOEWIM powered by two dual indirect matrix converters," *Energies*, vol. 14, no. 18, 2021, doi: 10.3390/en14185625.
- [19] S. Massoum, A. Meroufel, A. Massoum, and W. Patrice, "DTC based on SVM for induction motor sensorless drive with fuzzy sliding mode speed controller," *International Journal of Electrical and Computer Engineering*, vol. 11, no. 1, pp. 171–181, 2021, doi: 10.11591/ijece.v11i1.pp171-181.
- [20] H. Ziane, J. M. Retif, and T. Rekioua, "Fixed-switching-frequency DTC control for PM synchronous machine with minimum torque ripples," in *Canadian Journal of Electrical and Computer Engineering*, 2008, vol. 33, no. 3–4, pp. 183–189, doi: 10.1109/cjee.2008.4721636.
- [21] K. B. Lee and F. Blaabjerg, "An improved DTC-SVM method for sensorless matrix converter drives using an overmodulation strategy and a simple nonlinearity compensation," *IEEE Transactions on Industrial Electronics*, vol. 54, no. 6, pp. 3155–3166, 2007, doi: 10.1109/TIE.2007.905914.
- [22] U. R. Muduli, A. R. Beig, R. K. Behera, K. Al Jaafari, and J. Y. Alsawalhi, "Predictive Control with Battery Power Sharing Scheme for Dual Open-End-Winding Induction Motor Based Four-Wheel Drive Electric Vehicle," *IEEE Transactions on Industrial Electronics*, vol. 69, no. 6, pp. 5557–5568, 2022, doi: 10.1109/TIE.2021.3091919.
- [23] A. Berzoy, J. Rengifo, and O. Mohammed, "Fuzzy Predictive DTC of Induction Machines with Reduced Torque Ripple and High-Performance Operation," *IEEE Transactions on Power Electronics*, vol. 33, no. 3, pp. 2580–2587, 2018, doi: 10.1109/TPEL.2017.2690405.
- [24] A. Nasr, C. Gu, X. Wang, G. Buticchi, S. Bozhko, and C. Gerada, "Torque-Performance Improvement for Direct Torque-Controlled PMSM Drives Based on Duty-Ratio Regulation," *IEEE Transactions on Power Electronics*, vol. 37, no. 1, pp. 749–760, Jan. 2022, doi: 10.1109/TPEL.2021.3093344.
- [25] S. G. Petkar and V. K. Thippiripati, "A Novel Duty Controlled DTC of a Surface PMSM Drive With Reduced Torque and Flux Ripples," *IEEE Transactions on Industrial Electronics*, 2022, doi: 10.1109/TIE.2022.3181405.




- [26] M. Z. Aihsan, A. Jidin, A. Alias, S. A. A. Tarusan, Z. M. Tahir, and T. Sutikno, "Torque ripple minimization in direct torque control at low-speed operation using alternate switching technique," *International Journal of Power Electronics and Drive Systems*, vol. 13, no. 1, pp. 631–642, 2022, doi: 10.11591/IJPEDS.V13.I1.PP631-642.
- [27] M. A. Aazmi et al., "Direct torque control of induction motor with different energy storage for electrical vehicle (EV) application," in *Journal of Physics: Conference Series*, 2021, vol. 2107, no. 1, doi: 10.1088/1742-6596/2107/1/012052.
- [28] Y. P. Yang, J. J. Liu, T. J. Wang, K. C. Kuo, and P. E. Hsu, "An electric gearshift with ultracapacitors for the power train of an electric vehicle with a directly driven wheel motor," *IEEE Transactions on Vehicular Technology*, vol. 56, no. 5, pp. 2421–2431, 2007, doi: 10.1109/TVT.2007.899956.
- [29] Z. M. Tahir, A. Jidin, and M. L. M. Jamil, "Multi-carrier switching strategy for high-bandwidth potential balancing control of multilevel inverters," *International Journal of Power Electronics and Drive Systems*, vol. 12, no. 4, pp. 2384–2392, 2021, doi: 10.11591/ijpeds.v12.i4.pp2384-2392.
- [30] M. L. De Klerk and A. K. Saha, "A Comprehensive Review of Advanced Traction Motor Control Techniques Suitable for Electric Vehicle Applications," *IEEE Access*, vol. 9, pp. 125080–125108, 2021, doi: 10.1109/ACCESS.2021.3110736.

BIOGRAPHIES OF AUTHORS






Muhammad Zaid Aihsan    received the B.Eng. and M.Sc. degrees in Electrical Engineering from Universiti Malaysia Perlis, Malaysia, in 2013 and 2016, respectively. He is currently working on the Ph.D. degree under Power Electronics and Drives Research Group (PEDG) in the Faculty of Electrical Engineering, Universiti Teknikal Malaysia Melaka (UTeM), Malaysia. He is a Lecturer at Universiti Malaysia Perlis (UniMAP), Malaysia. His research interests include the power electronics and motor drive systems. He can be contacted at email: zaid@unimap.edu.my.






Auzani Jidin    received the B.Eng. degrees, M.Eng. degrees and Ph.D. degree in power electronics and drives from Universiti Teknologi Malaysia, Johor Bahru, Malaysia, in 2002, 2004 and 2011, respectively. He is currently an academician in Faculty of Electrical Engineering, Universiti Teknikal Malaysia Melaka, Melaka, Malaysia. He is also an active researcher in Power Electronics and Drives Research Group (PEDG) that established under the same faculty. His research interests include power electronics, motor drive systems, field-programmable gate array, and DSP applications. He can be contacted at email: auzani@utem.edu.my.



Azrita Alias    received her B. Eng in Electrical (Control and Instrumentation) (Hons) and M. Eng (Electrical) from the Universiti Teknologi Malaysia, in 2000 and 2003, respectively, and her PhD from University of Malaya in 2015. She is a senior lecturer at the Faculty of Electrical Engineering, Universiti Teknikal Malaysia Melaka (UTeM). Her main research interests are in modeling, control systems design and power electronics application in engineering systems. She can be contacted at email: azrita@utem.edu.my.



Tole Sutikno    is a Lecturer in Electrical Engineering Department at the Universitas Ahmad Dahlan (UAD), Yogyakarta, Indonesia. He received his B.Eng., M.Eng. and Ph.D. degree in Electrical Engineering from Universitas Diponegoro (Semarang, Indonesia), Universitas Gadjah Mada (Yogyakarta, Indonesia) and Universiti Teknologi Malaysia (Johor, Malaysia), in 1999, 2004 and 2016, respectively. He has been an Associate Professor in UAD, Yogyakarta, Indonesia since 2008. He is currently an Editor-in-Chief of the TELKOMNIKA, Director of LPPI UAD, and the Head of the Embedded Systems and Power Electronics Research Group. His research interests include the field of digital design, industrial electronics, industrial informatics, power electronics, motor drives, industrial applications, FPGA applications, artificial intelligence, intelligent control, embedded system and digital library. He can be contacted at email: tole@ee.uad.ac.id.